The effect of timescale separation on the tipping window for chaotically forced systems

Raphael Römer and Peter Ashwin

Department of Mathematics and Statistics,

University of Exeter, Exeter EX4 4QF, UK

April 18, 2025

Abstract

Tipping behaviour can occur when an equilibrium loses stability in response to a slowly varying parameter crossing a bifurcation threshold, or where noise drives a system from one attractor to another, or some combination of these effects. Similar behaviour can be expected when a multistable system is forced by a chaotic deterministic system rather than by noise. In this context, the chaotic tipping window was recently introduced and investigated for discrete-time dynamics. In this paper, we find tipping windows for continuous-time nonlinear systems forced by chaos. We characterise the tipping window in terms of forcing by unstable periodic orbits of the chaos, and we show how the location and structure of this window depend on the relative timescales between the forcing and the responding system. We illustrate this by finding tipping windows for two examples of coupled bistable ODEs forced with chaos. Additionally, we describe the dynamic tipping window in the setting of a changing system parameter.

Contents

1 Introduction

In many models of real-world systems, different processes can evolve over very different timescales. If one subsystem evolves chaotically on a rapid timescale and forces another slower subsystem, the faster subsystem can be seen as similar to a noise process driving the slower part. Conversely, if the forcing subsystem evolves much more slowly than the system it forces, then the system can be seen as a slowly varying parameter of the forced subsystem.

Such timescale separations allow for substantial simplifications of models for processes in a variety of applications from ecology, neuroscience, and chemistry to economics and data science; see for example [9, 18]. It is also a common assumption in climate modelling, made explicit by Hasselmann [15, 21], that weather processes are rapid and chaotic and that variability of climate variables (such as global mean surface temperature) occurs on a slower timescale driven by the weather fluctuations. This suggests that climate can be modelled using stochastic differential equations, where the chaotic driving is approximated by a white noise (Wiener process) driving.

Recent progress has shown that this is indeed the case for many systems in an appropriate limit [17, 14, 22]. In particular, if the fast dynamics are ergodic and exponentially rapidly mixing, homogenization theory [17, 22] gives a setting where this approximation is correct in the limit of the chaotic forcing subsystem being infinitely fast compared to the forced subsystem. Away from this limit, modeling fast dynamics as a noise process can clearly lead to even qualitatively wrong results; for example, if the chaotic forcing is bounded, there are some transitions between attractors that are possible in SDEs but not for bounded forcing.

This qualitative difference between chaotic and stochastic forcing can be seen when considering a bistable system forced by either a Wiener process or bounded chaos. Initialized close to one attractor forcing with a Wiener process will almost surely lead to tipping to the basin of attraction of the other attractor in finite time whose asymptotics are given by the Eyring-Kramers formula [9]. In contrast, bounded chaotic forcing does not necessarily lead to tipping at all. Even if the forced bistable system is close to a bifurcation, tipping will strongly depend on the realization of the chaotic forcing; some forcing trajectories might lead to tipping of the bistable system, but others might not.

This effect has been characterized as the appearance of a chaotic tipping window [5] near tipping points of systems that are chaotically forced. It is the region in the parameter space of a forced system for which it tips for some specific trajectory of a chaotic forcing but not for others. Outside the chaotic tipping window, the system will either never tip or always tip independently of the specific forcing trajectory. Note that the entrance into the chaotic tipping window can also be seen from the perspective of the full system

as a loss of stability of an attractor as a result of a crisis. The detailed example in [5] considered discrete time and a particularly simple chaotic forcing such that many results could be rigorously proven. In this paper, we consider the case of continuous-time ODEs; we analyze how varying the relative timescales affect these chaotic tipping windows.

In Section 2, we generalize the notion of the tipping window for a chaotically forced system independent of relative timescales. We derive analytical results in limiting cases of infinite timescale-separation, which we do in Section 2.1 for a one-dimensional system; in particular, we show that the extrema of the forcing are important to determine tipping in the case of slow forcing, while the mean of the forcing is important to determine tipping for the case of rapid periodic forcing.

In Section 3, we verify these results for two chaotically forced bistable ODE examples. The first is a double-well system where the bifurcation parameter is additively forced by the first variable of the Lorenz-63 system in the chaotic regime. The second is a Stommel system forced by Lorenz-63 in a similar way. We compute the tipping window of these systems when changing the relative speed between forcing and response by examining the response of the bistable systems to unstable periodic orbits (UPOs). We verify that in the limiting cases of timescale separation, indeed, the mean and extrema of the forcing UPOs allow us to determine the tipping window. For cases of intermediate relative timescales, there is a nontrivial rearrangement of the UPOs that determines the boundaries of the tipping window. We examine this for a specific example and find that there is a balance between the relative timescales and the duration that the UPOs can overshoot a bifurcation point.

In Section 4, we turn to the *dynamic tipping window* also introduced in [5]. This is a non-autonomous version of the tipping window, as the bifurcation parameter is now ramped at a finite rate. In the limit of infinitely slow parameter ramping, we limit to the tipping window of the autonomous case. We end with a brief discussion in Section 5.

1.1 Tipping points and chaotic forcing timescales

A *tipping event* occurs when a nonlinear system has a large or rapid change in state in response to small or slow changes in forcing. These events can happen in nonlinear systems as a result of various mechanisms [7, 6]. *Bifurcation tipping* (B-tipping) occurs when a system parameter slowly crosses a bifurcation point that results in the loss of any nearby attractor. *Rate-induced tipping* (R-tipping) can occur when parameter changes are fast enough that the adiabatic approximation breaks down. *Noise-induced tipping* (N-tipping) is another tipping mechanism that is usually studied in systems driven by Gaussian noise (i.e. a Wiener process), where unboundedness of the noise means that in the presence of two or more attractors there will almost surely be tipping between them on waiting a sufficiently long time. Non-trivial dynamics on the attractor may bring new effects such as *partial tipping* [2, 4], *phase tipping* [1]. In the presence of chaotic forcing, the *chaotic* and *dynamic tipping windows* [5] can appear.

Let us consider a forced nonlinear system in the timescale t of the response, inspired

by [5], where the forcing and response timescales have a ratio $\gamma > 0$, namely

$$
\begin{aligned}
\frac{dx}{dt} &= f(x, \eta(t), a\phi(y)) \\
\frac{dy}{dt} &= \gamma g(y)
\end{aligned}
\tag{1}
$$

with $x \in \mathbb{R}^d$, $y \in \mathbb{R}^n$, $\eta \in \mathbb{R}$, $\phi : \mathbb{R}^n \to \mathbb{R}$ and $a \geq 0$. We assume that f, η, ϕ and g are smooth functions of their arguments and a represents an amplitude of chaotic forcing $\phi(y)$ which is assumed to be bounded. We assume that f has B-tipping points of equilibria for the case $a = 0$ and slow variation of η. If we write the timescale of the forcing as $\tau = \gamma t$ then we can express (1) as

$$
\begin{aligned}
\frac{dx}{d\tau} &= \gamma^{-1} f(x, \eta(\gamma\tau), a\phi(y)) \\
\frac{dy}{d\tau} &= g(y).
\end{aligned}
\tag{2}
$$

The function $\eta(t)$ describes the values of the system parameters for any time t. We will assume that the y dynamics has a physical ergodic invariant measure m (i.e. a positive Lebesgue measure set of initial conditions has empirical measures that converge to m [26]) and we suppose that the initial condition $y(0)$ is typical with respect to this physical measure. If $\eta(t)$ is assumed to change on a time scale much slower than either x or y, then the dynamics of (1) can be largely understood in terms of the following *frozen system with chaotic forcing* (in terms of the response timescale) by fixing η:

$$
\begin{aligned}
\frac{dx}{dt} &= f(x, \eta, a\phi(y)) \\
\frac{dy}{dt} &= \gamma g(y).
\end{aligned}
\tag{3}
$$

We discuss in the next Section how a bifurcation for (3) with $a = 0$ can become a tipping window for $a > 0$ and how γ can influence the form of this tipping window.

2   The chaotic tipping window

For some forcing amplitude $a > 0$, the tipping window $W(a)$ characterizes the set of parameters η for which the system (3) undergoes tipping events for some realisations of the forcing but not for others. This concept was introduced in [5] and investigated there in the context of discrete dynamical systems. For clarity, we restrict (3) to a special case of an additively forced system for $x \in \mathbb{R}$ given by

$$
\begin{aligned}
\frac{dx}{dt} &= f(x) + \eta + a\phi(y) \\
\frac{dy}{dt} &= \gamma g(y).
\end{aligned}
\tag{4}
$$

where $\frac{dx}{dt} = f(x) + \eta$ is bistable for some values of η. Note that if that if $y(\tau)$ is a solution of

$$
\frac{dy}{d\tau} = g(y)
\tag{5}
$$

4

then (4) can be written as

$$\frac{dx}{dt} = f(x) + \eta + a\phi(y(\gamma t)). \tag{6}$$

Now, suppose that the unforced system

$$\frac{dx}{dt} = f(x) + \eta \tag{7}$$

has a bifurcation point η^* that can cause B-tipping. Specifically, suppose there are two attractors for some range $\eta^\dagger < \eta < \eta^*$ and only one attractor for $\eta > \eta^*$, and that one of the attractors disappears at a saddle-node bifurcation $\eta = \eta^*$.

Consider a small but positive forcing strength $a > 0$ for (6). In this context, the *chaotic tipping window* about η^* will be an interval $W(a)$ such that whenever $\eta \notin W(a)$, the system (6) has either one, or two attractors independent of the chosen forcing solution $y(\tau)$ of (5), and such that

$$\lim_{a \to 0} \sup\{d(x, \eta^*) \; : \; x \in W(a)\} = 0,$$

i.e. such that both endpoints of the interval $W(a)$ limit to η^* for $a \to 0$.

Within the chaotic tipping window, i.e. for $\eta \in W(a)$, the dynamics of the full system (6) will depend on the specific trajectory of the chaotic forcing (5). For some forcing trajectories of the chaotic system (5) there is only one attractor for (6): the chaotically forced system tips earlier than the unforced system (7) would have tipped as a result of adiabatically varying η. Other trajectories of the chaotic system (5) will give more than one attractor for the system (6): the chaotically forced system tips later than the unforced system (7) would have tipped as a result of adiabatically varying η.

The chaotic tipping window $W(a)$ can be introduced analogously to [5]. Consider the set $\mathcal{S}(m)$ of all ergodic invariant measures for the y-dynamics that are supported within the support of the physical measure m. We write $\mathcal{P}(m)$ to denote the unstable periodic orbits within the attractor; clearly $\mathcal{P}(m) \subset \mathcal{S}(m)$. We introduced the notion that the system has one attractor when forced by $s \in \mathcal{S}(m)$ if there is a full measure set of trajectories y w.r.t. s such that (3) has only one attractor for x. Following [5], for fixed parameters we define the set

$$M(s, a) := \{\eta \; : \; \text{the system for given } a \text{ has one attractor when forced by } s \in \mathcal{S}(m)\},$$

and the set of chaotic tipping windows as

$$W(a) := \{\eta \; : \; \eta \in M(s, a) \cap M^c(s', a) \;\; \text{for some } s, s' \in \mathcal{S}(m)\}.$$

As [5] notes, these correspond to those parameter values where different forcing trajectories may give a different number of attractors. In the case where $M(s, a)$ is a semi-infinite interval $(\eta_c(s, a), \infty)$ for all $s \in \mathcal{S}(m)$ the chaotic tipping window will be an interval $W(a) = [\eta_-(a), \eta_+(a)]$. The endpoints

$$\begin{aligned}
\eta_-(a) &= \inf\{\eta_c(s, a) \; : \; s \in \mathcal{S}(m)\}, \\
\eta_+(a) &= \sup\{\eta_c(s, a) \; : \; s \in \mathcal{S}(m)\}
\end{aligned} \tag{8}$$

of this window can be thought of as solving a problem of ergodic optimization. Measures realizing these extremes are often found to be periodic [16]; this was the case in [5], but here we find that this is not always the case. In [5] it was found that $\eta_c(s, a)$ is not simply an averaged observable but the boundary of a region of multistability, and it is not obvious how to generalize these results. The threshold on entry to the chaotic tipping window can also be understood in terms of a *non-autonomous saddle-node bifurcation* [3] of the non-autonomous system (6).

2.1   Tipping windows at the limits of timescale separation

Recall that τ is the timescale of the forcing $y(\tau)$, t is the timescale of the response $x(t)$, and $\tau = \gamma t$. Assume that for $a = 0$ there is a bifurcation at η^* in increasing η. In this section, we argue that the two limits of timescale separation, $\gamma \to 0$ and $\gamma \to \infty$, can be solved.

In the limit $\gamma \to 0$, the forcing evolves slowly compared to the forced system (7), and thus, the latter "sees" the instantaneous forcing. The tipping point is passed if $\eta + a\phi(y(\tau))$ exceeds η^* at any time, i.e. the critical η is at:

$$\eta_c(s, a) = \eta^* - a \sup\{\phi(y) \ : \ y \in \text{supp}(s)\}.$$

Hence the lower and upper bounds of the chaotic tipping window (8) will be given by

$$\begin{aligned} \eta_-(a) &= \eta^* - a \sup\left\{\sup\{\phi(y) \ : \ y \in \text{supp}(s)\} \ : \ s \in \mathcal{S}(m)\right\}, \\ \eta_+(a) &= \eta^* - a \inf\left\{\sup\{\phi(y) \ : \ y \in \text{supp}(s)\} \ : \ s \in \mathcal{S}(m)\right\}. \end{aligned} \tag{9}$$

In the limit $\gamma \to \infty$, the forcing evolves rapidly compared to the system of interest, and thus the latter only "sees" the mean value of the forcing: the tipping point is passed if $\eta + a\phi(y(\tau))$ exceeds η^* on average. In this case we argue that the lower and upper bounds of the chaotic tipping window will be given by the trajectories $s \in \mathcal{S}(m)$ whose mean values are maximal or minimal:

$$\begin{aligned} \eta_-(a) &= \eta^* - a \sup\left\{\int_y \phi(y)\, ds(y) \ : \ s \in \mathcal{S}(m)\right\}, \\ \eta_+(a) &= \eta^* - a \inf\left\{\int_y \phi(y)\, ds(y) \ : \ s \in \mathcal{S}(m)\right\}. \end{aligned} \tag{10}$$

We prove these statements in the $\gamma \to \infty$ case if $y(\tau)$ is an unstable periodic orbit within the chaotic attractor. For intermediate timescale ratio γ, deriving analytical results for the location of the attractor crisis will be non-trivial. We explore this numerically in Section 3 for a specific system of the form (6).

For a trajectory $y(\tau)$, we define

$$\widetilde{\Phi}(\tau) := \phi(y(\tau)),$$

write

$$\overline{\Phi} := \lim_{T \to \infty} \frac{1}{T} \int_{\tau=0}^{T} \phi(y(\tau))$$

(so that $\widetilde{\Phi}(\tau) = \overline{\Phi} + \Phi(\tau)$ with $\Phi(\tau)$ having zero mean), and define

$$\Phi^+ := \max_{\tau > 0} \phi(y(\tau)).$$

Theorem 2.1. *Suppose that (6) with $a = 0$ has a saddle-node bifurcation at η^* and at most two attractors, all of which are equilibria. Suppose that $y(\tau)$ is a solution of (5).*

(a) For sufficiently small $a > 0$ and in the limit $\gamma \to 0$ there is a tipping point at

$$\eta_c = \eta^* - a\Phi^+.$$

(b) If $y(\tau)$ is a UPO then for sufficiently small $a > 0$ and in the limit $\gamma \to \infty$ there is a tipping point at

$$\eta_c = \eta^* - a\overline{\Phi}.$$

Proof. The system (6) can be written as

$$\frac{dx}{dt} = f(x) + \eta + a\widetilde{\Phi}(\gamma t). \tag{11}$$

Suppose that the saddle-node bifurcation at $\eta = \eta^*$ for $a = 0$ has a hyperbolic attracting equilibrium $X(\eta)$ for $\eta^\dagger < \eta < \eta^*$. In case (a), we can view this as a two timescale system

$$\frac{dx}{dt} = f(x) + \eta + a\widetilde{\Phi}(s)$$
$$\frac{ds}{dt} = \gamma \tag{12}$$

which, in the singular limit $\gamma \to 0$ will have a critical set $\eta + a\widetilde{\Phi}(s) = -f(x)$ with fold at $\eta + a\widetilde{\Phi}(s) = \eta^*$. If $\eta^\dagger < \eta + a\widetilde{\Phi}(s) < \eta^*$ for all s (which is the case for some choices of η if a is small enough), then this will be linearly stable for the fast system. This will pass a tipping point if $\eta + a\Phi^+ = \eta^*$, hence the stated result for (a) that there is a tipping point at $\eta_c = \eta^* - a\Phi^+$.

In case (b), we can adapt the proof of the averaging theorem in [18, Chapter 9.6]. Note that we can write

$$\frac{dx}{dt} = f(x) + \eta + a\overline{\Phi} + a\Phi(\gamma t). \tag{13}$$

where Φ has zero mean. We define $\eta_a := \eta + a\overline{\Phi}$ and suppose that (13) has a stable equilibrium $x_0 = \bar{x} + z$. We linearize as

$$\frac{dz}{d\tau} = Lz + a\Phi(\gamma\tau) + O(|z|^2), \tag{14}$$

such that $L = \partial f/\partial x(\bar{x}, \eta_a) < 0$. We can solve the equation (14) truncated at linear terms only using the ansatz $z(t) = c(t)e^{Lt}$ so that

$$\frac{dz}{dt} = Lz + a\Phi(\gamma t) = Lz + \dot{c}(t)e^{Lt}$$
$$\Rightarrow \dot{c}(t) = a\Phi(\gamma t)e^{-Lt} \tag{15}$$
$$\Rightarrow c(\tau) = c_{-\infty} + \int_{-\infty}^{t} a\Phi(\gamma s)e^{-Ls}ds.$$

The solution to the linearized system is given by

$$z(t) = c_{-\infty}e^{Lt} + \int_{-\infty}^{t} a\Phi(\gamma s)e^{-L(s-t)}ds. \tag{16}$$

The corresponding pullback attracting solution is given by setting $c_{-\infty} = 0$, i.e. the unique uniformly bounded solution

$$z(t) = \int_{-\infty}^{t} a\Phi(\gamma s)e^{-L(s-t)} \, ds$$

$$= \frac{a}{\gamma} \int_{-\infty}^{0} \Phi(\gamma t + u)e^{-u\frac{L}{\gamma}} \, du. \tag{17}$$

Note that in the case $\gamma \to \infty$, this is the zero-decay limit of the Laplace transform with respect to u for the zero-mean periodic function $\Phi(\gamma t + u)$. This means that the response $\sup_t |z(t)| \to 0$ as $\gamma \to \infty$ and so the quadratic terms in (14) will be a higher order correction, as long as $L < 0$. For small $a > 0$, this will break down if $\eta + a\overline{\Phi} = \eta^*$. Hence the result (b) that there is a tipping point at $\eta_c = \eta^* - a\overline{\Phi}$ in this limit. $\qquad\square$

It should be possible to show an analogous result in the case where $y(\tau)$ is quasiperiodic or almost periodic in the sense that it is generic for a uniquely ergodic measure supported within the chaotic attractor, and where x is higher dimensional with Jacobian Df linearly stable, or when it is in a more general form than (3).

We can characterize the bounds of the chaotic tipping windows by considering unstable periodic orbits if these approximate invariant measures supported within the attractor [11]. For convenience, we will assume that this is the case for the chaotic attractors we consider and moreover that the basin of attraction of each UPO is dense in the basin of attraction of the chaotic attractor. If this is the case then we can compute $\eta_{\pm}(a)$ by considering only UPOs $s \in \mathcal{P}(m)$.

3 Tipping windows for bistable ODEs forced with chaos

In the previous section, we gave some results for a one-dimensional multistable system forced by a chaotic system in the limits of timescale separation. We now consider two examples to verify the results above and to extend them to cases of arbitrary timescale ratio.

3.1 Example I: 1D-double-well system forced by Lorenz-63

We consider a one-dimensional double-well potential system driven by trajectories on the Lorenz-63 attractor. The equations of the form (4) for $x \in \mathbb{R}$ and $y \in \mathbb{R}^3$ are:

$$\left.\begin{array}{l} \dfrac{d}{dt}x = f(x) + \eta + a\phi(y) \\[2mm] \dfrac{d}{dt}y = \gamma g(y) \end{array}\right\} \tag{18}$$

with $f(x)$ given by the dynamics in a double well potential

$$f(x) = 3x - x^3, \tag{19}$$

and $\phi(y) = y_1$ defined as the projection onto the first coordinate of the y-dynamics which are given by the Lorenz-63 system:

$$\left.\begin{aligned}g_1(y) &:= \sigma(y_2 - y_1)\\g_2(y) &:= y_1(\rho - y_3) - y_2\\g_3(y) &:= y_1 y_2 - \beta y_3.\end{aligned}\right\}. \tag{20}$$

The right-hand side of the x-dynamics of (18) can be written as the negative gradient of the η-dependent double-well potential

$$\bar{F}(x, \eta) = \frac{1}{4}x^4 - \frac{3}{2}x^2 - \eta x \tag{21}$$

driven by additive forcing ay_1. For $\eta = 0$, the unforced x-dynamics ($a = 0$) has two stable equilibria in $x_\pm = \pm\sqrt{3}$, and an unstable equilibrium at $x_s = 0$.

More generally, for $\eta \neq \pm 2$, the number and stability of the equilibria are as follows. For $\eta < -2$ there is 1 stable equilibrium $x_-(\eta) < -2$. For $-2 < \eta < 2$ there are 2 stable equilibria $x_+(\eta) \in (1, 2)$ and $x_-(\eta) \in (-2, -1)$ separated by 1 unstable equilibrium $-1 < x_s(\eta) < 1$. For $\eta > 2$ there is 1 stable equilibrium $x_+(\eta) > 2$. At $\lambda = \pm 2$ there are saddle-node (fold) bifurcations where $x_\pm(\eta)$ meets $x_s(\eta)$ and both disappear on passing through $\lambda = \pm 2$. Note that the location of the equilibria depends on η.

Turning to cases with $a > 0$, the y-dynamics become important. Initializing the x-dynamics in $x_0 < x_-(\eta)$ (i.e. in the basin of the attractor $x_-(\eta)$), setting $0 < a \ll 1$, and choosing different initial conditions of the y-dynamics close to the Lorenz-63 attractor, shows tipping to $x_+(\eta)$ depending on the exact initial condition of the forcing y_0, the value of η, and the value of γ.

Figure 1 shows some typical trajectories for three different choices of η. The behaviour of the orange trajectories suggests that this value of η lies within the tipping window defined in Section 2, since some trajectories tip and others do not tip within the integration time. In contrast, all green trajectories tip immediately and no blue trajectories tip within the given time, suggesting that the associated η-values are not in the tipping window. Computing the exact location of the tipping window is however far from trivial, as it involves exploring a large set of untypical trajectories on the Lorenz attractor that yield the most extreme behaviour on forcing.

A typical chaotic attractor will support an infinite number of unstable periodic orbits (UPOs) [24, 10], and the set of periodic orbits will be dense on the attractor. Thus, understanding response of a system forced by UPOs on the same attractor will help to understand the dynamics of that system forced by more general trajectories on the Lorenz attractor. In particular, any orbit can be approximated by switching between UPOs. Moreover, almost every chaotic orbit will shadow every UPO for an arbitrarily long time. As discussed in [16], UPOs support ergodic measures that often realise extreme behaviour in a typical forced system.

We compute UPOs on the Lorenz attractor as described in the Appendix A for the subsequent analysis. A collection of them is shown in Figure 11 and some basic characteristics of these orbits are listed in Table 3. In the next sections, we use these UPOs to explore the tipping window for a range of timescale ratios γ.
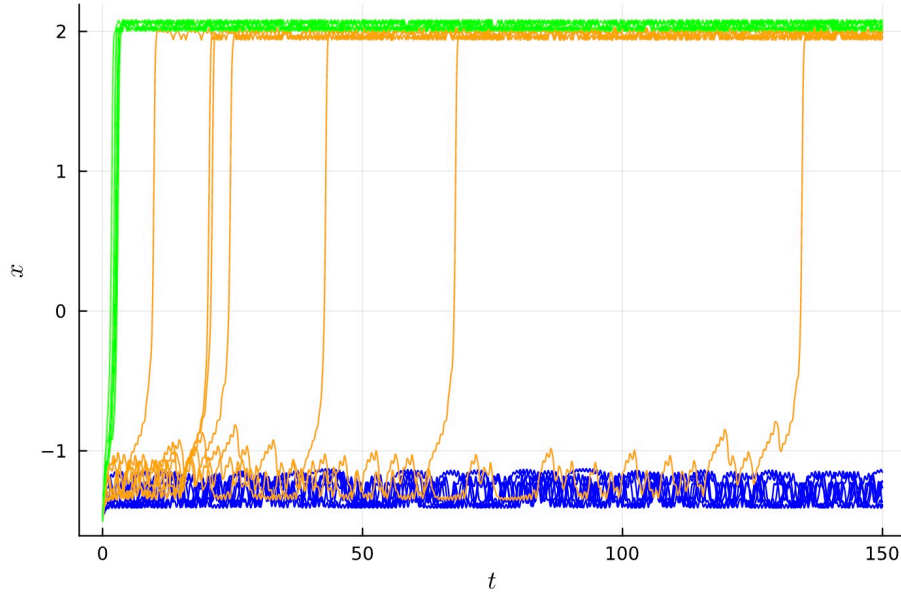
9

Figure 1: Typical trajectories of the Lorenz-double-well system with $a = 0.03$, $\gamma = 1$, randomly chosen initial conditions of the Lorenz-y-dynamics, and three different values of η. The x-dynamics are initialized at $x = -1.5$ in the basin of attraction of the double-well attractor $x_-(\eta)$. The blue curves ($\eta = 1.7$) remain in the vicinity of the attractor of the x-dynamics they started in. The orange curves ($\eta = 1.85$) show tipping within the given time depending on the specific y-trajectory. The green curves ($\eta = 2.01$) always tip independently of the specific Lorenz trajectory. The y-trajectories are generated by taking the final state of the previous ensemble member as the initial condition for the next.
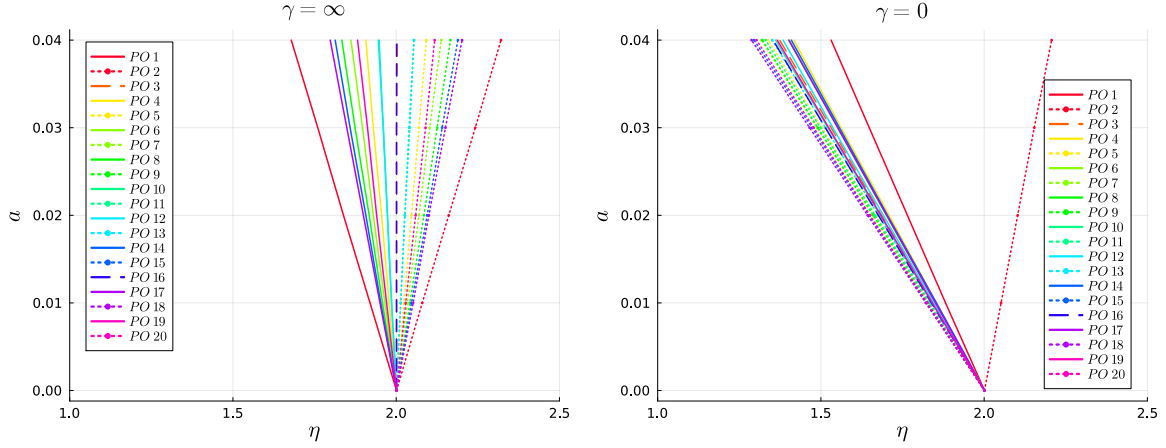
Figure 2: The coloured lines show for each a the lowest value of η for which tipping is observed when forcing the double-well system (23) with the mean (left plot) or the maximum (right plot) of the colour-coded UPO. The system is of the form of equation (6) with $\phi(y(\gamma t)) = \bar{y}_{1,UPO_k}$ given by the mean (left plot) or $\phi(y(\gamma t)) = \max(y_{1,UPO_k})$ the maximum (right plot) of the k-th UPO. For each UPO, we fix discrete values of $a \in [0, 0.04]$ with spacing of 0.01 and then do bisections in $\eta \in (0.4, 1.6)$ to approximate the lowest η up to an accuracy of 5×10^{-3} for which the system, initialized in $x = -1.5$, tips to the positive equilibrium, i.e. $x > 0$. Note that in the left plot, the lines are ordered from left to right by decreasing mean y_1-value of the associated UPOs, and each line is given by $\eta_k(a) = \eta^* - a\bar{y}_{1,UPO_k}$ as derived in section 2.1. In the right plot, the lines are ordered from left to right by decreasing maximum y_1-value of the associated UPOs, and each line is given by $\eta_k(a) = \eta^* - a\max(y_{1,UPO_k})$.

3.1.1 The tipping window for limiting timescale separations

As described in Theorem 2.1, in the limit of infinite timescale separation, the UPO forcing of the form considered here limits to a constant additive shift of the bifurcation parameter η. The location of the bifurcation then depends on the forcing strength a and is given by that Theorem.

We plot the bifurcation location for each of the 20 UPOs for both limits of infinite timescale separation in Figure 2. As expected, the location of the bifurcation depends linearly on a.

For $\gamma \to \infty$, the y-dynamics are infinitely faster than the x-dynamics and Theorem 2.1 means that the lines are ordered by their mean value $\bar{y}_1$. Forcing the Stommel system by symmetric UPOs 3 and 18 resulted in the dashed lines which all lie on top of each other because they all have the same mean $y_1 = 0$. The lines of the symmetric periodic orbits are mirrored along the axis $\eta = 0$.

For the limit $\gamma \to 0$, the lines are ordered by their maximum value $\max(y_1)$. Forcing by symmetric UPOs now does not result in the same dashed line since the symmetric UPOs can have different maximal y_1 values. In addition, the lines of the rotated periodic orbits are no longer mirrored along a line. Note that even though the lines of the 1st and 2nd UPOs are seemingly in the same positions as for $\gamma = \infty$, they slightly shifted since they are now dependent on the maximum $\max(y_1)$ along the UPOs whereas they were given by the mean $\bar{y}_1$ for $\gamma = \infty$.

11

3.1.2 The tipping window for intermediate timescale ratios

Now, we would like to understand the tipping window for cases other than limiting timescale separation. We simulate for four different values of the timescale parameter γ, forcing the double-well system with a) the UPOs from Figure 11 and b) with randomly chosen non-periodic chaotic trajectories on the Lorenz attractor. Note that care needs to be taken that the slowest system is integrated for a sufficiently long duration.

Figure 3 shows these results in a similar way to Figure 2: for the coloured curves we choose a range of different forcing amplitudes $a \in [0, 0.04]$, do a bisection in η to find the best approximation of the lowest η that leads to tipping to the positive attractor $x_+(\eta)$, and consider a set of different values of the timescale parameter $\gamma \in (0.01, 0.1, 1, 10)$ in the four panels.

On the same figure, for a grid of a and η values, we run one simulation per grid point with the x-dynamics initialized in $x = -1.5$ which is in the basin of attraction of $x_-(\eta)$ if this attractor exists for the given value of η, and the y-dynamics initialized randomly close to the attractor with an initial transient removed. Then we monitor whether the trajectory tips to the other attractor $x_+(\eta)$ and, if so, at which time.

Interpreting each of the four plots for different γ in Figure 3 can be done by fixing a forcing strength a. For small η, we do not observe tipping within the given time t_{max} (black area). The larger η, the shorter the observed tipping times. The right end of the black area tilts to the left for smaller γ. We see that the cases $\gamma = 0.01$ and $\gamma = 10$ approximate well the limiting cases shown in Figure 2. For intermediate γ, a rather smooth interpolation between the two limiting cases can be seen. Note that for $\gamma = 0.01$ some chaotically forced trajectories tipped during the given simulation time for η smaller than the leftmost UPO line. This is not observed for large γ. The fact that this only occurs for small γ means that for small γ, chaotic forcing can lead to a more extreme forcing scenario than UPO forcing and vice versa for large γ. This can be expected:

- For γ small, the maximal y_1-values along the entire length of the orbit determine the extremeness of the forcing. A randomly chosen long chaotic trajectory on the Lorenz attractor is likely to assume larger values of y_1, and thus earlier tipping than one of the 20 UPOs used in this paper.

- For γ large, the mean of the forcing trajectory is the relevant quantity. As the mean of a randomly chosen chaotic Lorenz trajectory is likely to be close to zero, more extreme forcing can be seen from UPO forcing as they are very unusual trajectories with mean bound away from zero if they are asymmetric.

The second point also implies that the upper bound of the tipping window can be better approximated with the UPOs for large γ as some UPO forcing trajectories can have a large negative mean value of y_1 and thus lead to tipping for unusually large η. In contrast, it is unlikely to find long chaotic forcing trajectories that stabilize the system enough to not tip for large η.

The upper bound of the tipping window for γ small is also unlikely to be well approximated by a randomly chosen chaotic forcing trajectory, as such a chaotic trajectory is unlikely to have a maximal y_1 that is smaller than the maximal y_1s of every single UPO. In fact, UPO2 only explores a subset of the negative wing of the Lorenz attractor, and some of the other UPOs do not explore large positive values of the positive wing of the

γ	white	lightgray	darkgray	black
0.01	$[0,\ 0.0175)$	$[0.0175,\ 0.05)$	$[0.05,\ 150)$	$[150,\ \infty)$
0.1	$[0,\ 0.12)$	$[0.12,\ 0.5)$	$[0.5,\ 150)$	$[150,\ \infty)$
1	$[0,\ 1.25)$	$[1.25,\ 3.0)$	$[3.0,\ 150)$	$[150,\ \infty)$
10	$[0,\ 12)$	$[12,\ 20)$	$[20,\ 150)$	$[150,\ \infty)$

Table 1: Time intervals used to determine tipping for each of the different gray shadings in Figure 3; if a randomly chosen initial condition for y results in tipping in the corresponding time interval then the shading is used, otherwise we used black to indicate the tipping has not occurred by time 150.

Lorenz attractor. Thus, the only case where chaotic forcing should be used to approximate the boundary of a tipping window is the lower bound of the tipping window for small γ.

As discussed in Section 2.1, in the limit of infinitely fast periodic forcing, the forced system only sees the mean of the forcing. In the opposite limit, the forcing is given by just the initial condition of the periodic orbit. When fixing the forcing strength to some value $a = 0.04$, we can plot γ vs. η and see how the intermediate cases interpolate between the limits of infinite timescale separation shown in Figure 4.

3.1.3 Crossing of UPO lines and the lower bound of the tipping window

In Figure 3, we can see that for $\gamma = 0.1$, the lines resulting from forcing with UPOs 3 to 20 cross the UPO1 line. The location of the crossing points of each single UPO3-20 line with the UPO1 line depends on a, η, and γ. We approximate the location of the crossing point of the UPO1 and UPO4 lines by checking the intersection of the UPO4 line with the line given by $\eta(a) = \eta^* - \frac{a}{2}(\max(y_{1,UPO_1}) + \bar{y}_{1,UPO1})$. This line lies exactly between the UPO1 lines of the limiting cases $\gamma = 0$ and $\gamma = \infty$ and is thus an approximation of the UPO1 line. Figure 5 shows that the location in a where UPO1 and UPO4 cross is approximately scaling quadratically in γ.

This seems reasonable because of the following. For intermediate timescale ratios, the forcing by a UPO may overshoot the threshold η for a short time, and as long as this is not too long relative to the time spent below the threshold, the system may still not tip.

In this context, we note that an inverse square law determines whether a temporary overshoot over a fold bifurcation leads to tipping to the other attractor or not [23]; this is given by $Rt_{over}^2 < \kappa$ with R the maximal value of the overshoot, t_{over} the total time during which the parameter is larger than the bifurcation value, and $\kappa \in \mathbb{R}$ a constant plus an additive correction of the order of the timescale of the parameter ramping. By using the relation $\eta(a) = \eta^* - \frac{a}{2}(\max(y_{1,UPO_1}) + \bar{y}_{1,UPO1})$, we can assume the overshoot time t_{over} to be inversely proportional to γ and the maximal overshoot distance R to be proportional to the forcing amplitude a. This suggests that the critical value of a scales as $a \approx \kappa\gamma^2$ which agrees well with the numerics shown in Figure 5.
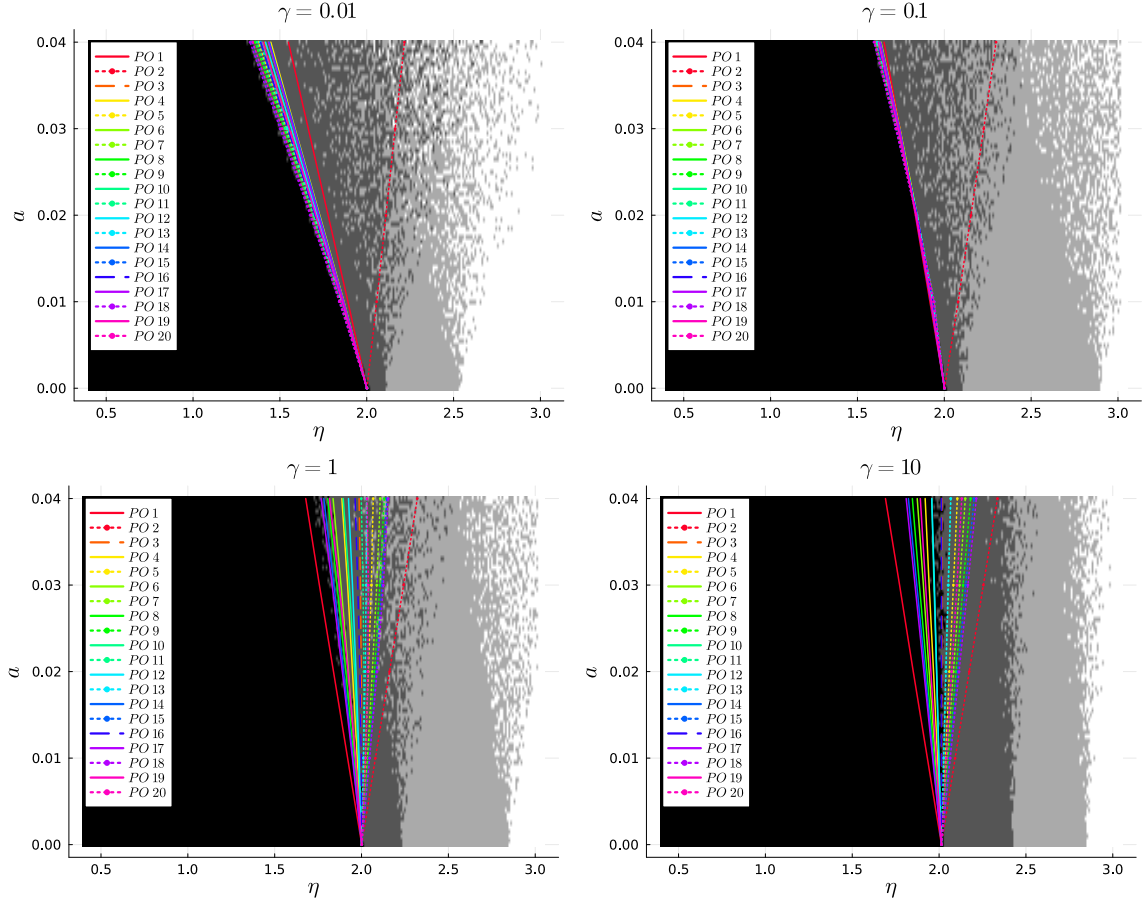
Figure 3: The coloured lines show for each a the lowest value of η for which tipping is observed when forcing the double well system (23) with the colour-coded UPO. The system is of the form of equation (6) with $y_1(t) = y_{1,UPO_k}$ given by the kth UPO and $\gamma \in (0.01, 0.1, 1, 10)$. For each UPO, we fix discrete values of $a \in [0, 0.04]$ with spacing 0.01 and then do bisections in $\eta \in (0.4, 1.6)$ to approximate the lowest η up to an accuracy of 5×10^{-3} for which the system initialized in $x = -1.5$ tips to the positive attractor i.e. $x > 0$. The black, dark gray, light gray, and white shading show in which time interval tipping of the double-well system 19 initialized in the basin of the attractor $x_-(\eta)$ (at $x = -1.5$), was observed as a result of forcing with a randomly chosen Lorenz-trajectory. The Lorenz-initial condition of one run is given by letting the final condition of the previous run evolve for 5 Lorenz-timesteps. The first initial condition of the Lorenz system is given by starting the system at $(y_1, y_2, y_3) = (0.1, 0.1, 25.1)$ and letting it relax to the attractor for 5 Lorenz-timesteps. In the white areas tipping to the other attractor $x_+(\eta)$ was observed at a very small time, and in black areas, tipping was not observed at all during the simulation time. The gray shadings showed tipping for intermediate times. The time-intervals corresponding to the different shading colours are given in Table 1 for each value of γ.
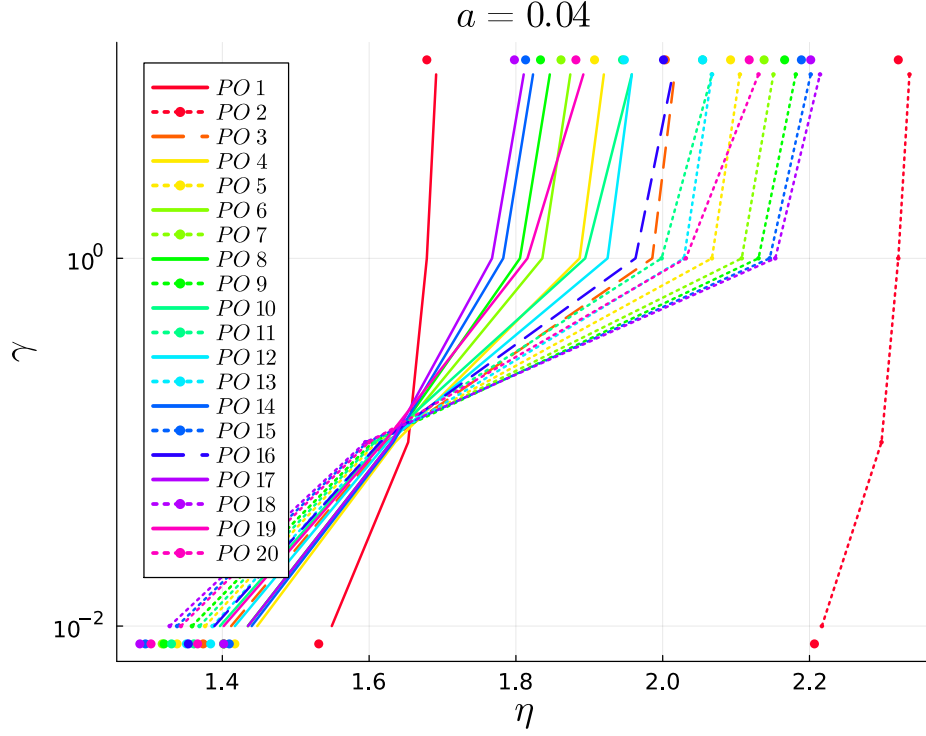
Figure 4: For fixed $a = 0.04$, we plot the critical values of η from Figure 3 vs. γ. The dots at the top and bottom show the location of the tipping point for the limiting cases of timescale separation. 3
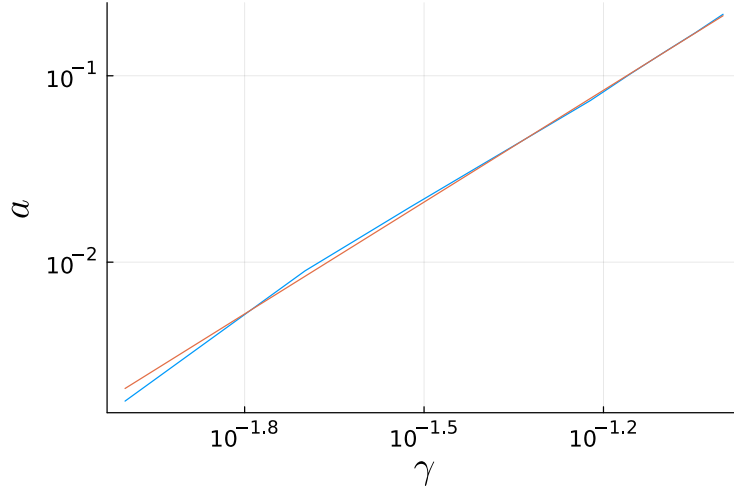

Figure 5: We do a bisection in a for a set of fixed $\gamma \in \{0.01, 0.02, \ldots, 0.1\}$ to find the smallest value of a such that tipping in response to UPO4 forcing occurs earlier than tipping in response to UPO1 forcing; more precisely we compare the tipping η for UPO4 with $\eta(a) = \eta^* - \frac{a}{2}(\max(y_{1,UPO_1}) + \bar{y}_{1,UPO_1})$ to find the lowest a as a function of γ, shown here on a log-log plot. The orange line corresponds to the fit $a = 21\gamma^2$.

3.2 Example II: 2D-Stommel model forced by the Lorenz-63 system

Our analysis so far has been concerned with the case of a one-dimensional system forced by a one-dimensional projection of a chaotic system. In most real-world applications the system that gets forced by another chaotic system is higher-dimensional,though. In this section, we explore a simple two-dimensional model inspired by climate science to check that the qualitative conclusions also apply in a higher-dimensional system.

The system described in [4] consists of a Lorenz-63 system forcing a Stommel model, which is a strongly reduced model of the Atlantic meridional overturning circulation (AMOC) [25]. The two state variables $x \in \mathbb{R}^2$ describe the salinity and temperature difference between two ocean regions [13]. We consider the typical Lorenz-63 parameters in the chaotic regime. The forcing of the Stommel system can be seen as a simple way of modelling internal variability. Note that we do not claim the considered parameters and model architecture to be of direct relevance to the AMOC. The Lorenz model can be viewed as a generic and bounded chaotic forcing of the Stommel model; the timescales may or may not be separated depending on the choice of γ. The model equations for $x = (x_1, x_2)$ and $y = (y_1, y_2, y_3)$ are given by

$$\left.\begin{aligned} \frac{d}{dt}x &= f(x, \xi_1 + ay_1, \eta_1 + ay_1) \\ \frac{d}{dt}y &= \gamma g(y) \end{aligned}\right\} \tag{22}$$

where the Stommel right hand side is

$$\left.\begin{aligned} f_1(x, \xi, \tilde{\eta}) &:= -x_1(1 + |x_1 - x_2|) + \xi \\ f_2(x, \xi, \tilde{\eta}) &:= -x_2(\zeta + |x_1 - x_2|) + \eta \end{aligned}\right\} \tag{23}$$

and the Lorenz right hand side is

$$\left.\begin{aligned} g_1(y) &:= \sigma(y_2 - y_1) \\ g_2(y) &:= y_1(\rho - y_3) - y_2 \\ g_3(y) &:= y_1 y_2 - \beta y_3. \end{aligned}\right\} \tag{24}$$

The timescale t is that of the response system (6). The default parameters we use are:

$$\xi_1 = 3 \quad \zeta = 0.3, \quad \eta_1 \in [0, 1.8] \quad \sigma = 10, \quad \rho = 28, \quad \beta = 8/3 \tag{25}$$

and we vary γ, a and η_1 in the numerical experiments.

In this model, the AMOC-strength can be defined as the difference of the Stommel variables as

$$\Psi = x_1 - x_2. \tag{26}$$

The unforced Stommel model (23) (i.e. the x-dynamics from (22) with $a = 0$) has a stable attractor, the AMOC-on state with large $\Psi_+(\eta)$ for $\eta < \eta^*$, a saddle-node bifurcation on increasing η at $\eta^* \approx 1.22$ and for $\eta > \eta^*$, the system has only one attractor, the AMOC-off state with small $\Psi_-(\eta)$. We remark that [8] study attractor crises in this model, though
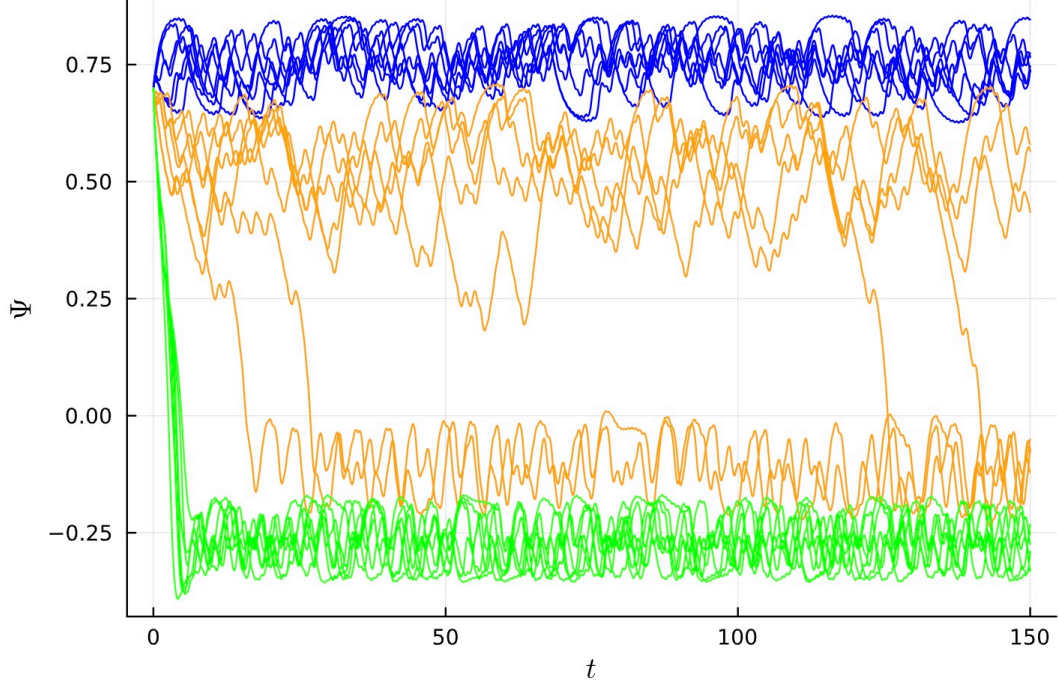
Figure 6: Typical trajectories of the Lorenz-Stommel system (22) with $a = 0.04$, $\gamma = 1$, randomly chosen initial conditions of the Lorenz-y-dynamics, and three different values of η_1. The x-dynamics are initialized in the vicinity of the AMOC-on attractor at $(x_1, x_2) = (1.7, 1.0)$. The blue curves ($\eta_1 = 1.0$) remain in the vicinity of the on-attractor. The orange curves ($\eta_1 = 1.175$) show tipping within the given time depending on the specific y-trajectory. The green curves ($\eta_1 = 1.5$) all tip independently of the specific Lorenz trajectory. The y-trajectories are generated by taking the final state of the previous ensemble member as the initial condition for the next one.

they do not consider the effect of varying the timescale ratio between forcing and response system.

For $a > 0$ the Stommel system is forced by the first chaotic variable and so we are in the setting (6). Note that the forcing does not only act on the bifurcation parameter η_1, but also on the dynamics of the first Stommel variable. In figure 6, we see typical trajectories showing the AMOC-strength.

To approximate the chaotic tipping window, we need to understand for which values of a and η_1 the system initialized in the basin of the AMOC-on state undergoes tipping to the AMOC-off state. Therefore, we perform simulations similar to those in Section 3.1 both for limiting timescale separation and intermediate timescale ratios.

3.2.1 The tipping window for limiting timescale separations

First, we consider the two limiting cases of infinite timescale separation $\gamma = 0$ and $\gamma = \infty$. We initialize the system in the vicinity of the AMOC-on state and force it with either the means of the first UPO coordinates (for $\gamma = \infty$) or with the maxima of the first UPO coordinates (for $\gamma = 0$) and do a bisection in η_1 to find the lowest for which the system tips. The results are shown in Figure 7. We observe a very similar behavior to the case of
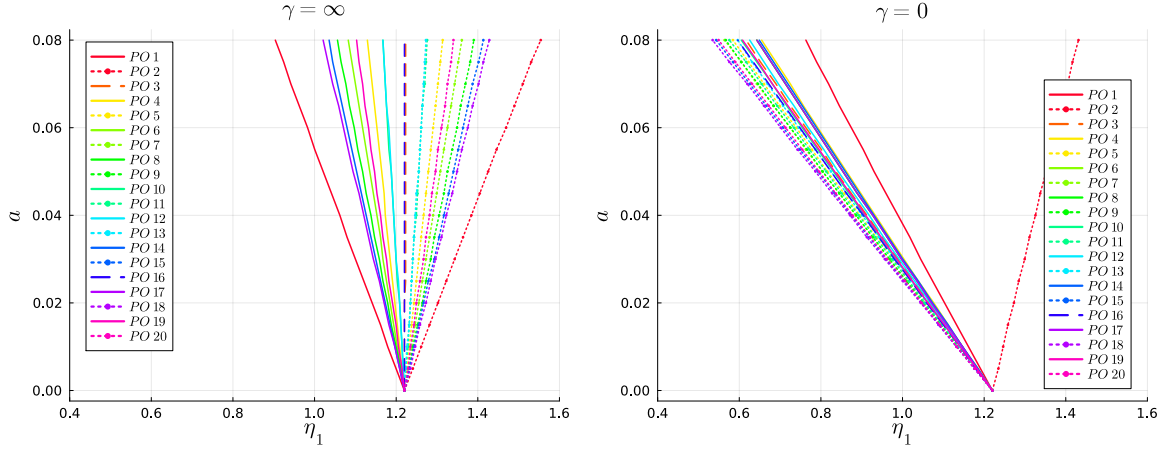
Figure 7: The coloured lines show for each a the lowest value of η_1 for which tipping is observed when forcing the Stommel system (22) with the mean $\bar{y}_{1,UPO_k}$ (left panel) or with the maximum $\max(y_{1,UPO_k})$ (right panel) of the first component of a colour-coded UPO from the Lorenz system. For each UPO, we fix discrete values of $a \in [0, 0.08]$ with spacing 0.01 and then perform bisections in $\eta_1 \in (0.4, 1.6)$ to approximate the lowest η_1 up to an accuracy of 5×10^{-3} for which the system initialized in the vicinity of the AMOC-on state at $(x_1, x_2) = (1.7, 1.0)$, tips to the AMOC-off state, i.e. $\Psi < 0.1$. Note the similarity to Figure 2.

the double-well system shown in Figure 2.

3.2.2 The tipping window for intermediate timescale ratios

Now, we turn to cases of intermediate timescale ratio. Again, these simulations are performed similarly to those described in Section 3.1. We run the system on a grid of $a \in (0, 0.08)$ and $\eta_1 \in (1, 1.5)$, always choose the initial condition of the Stommel system 23 to be in the vicinity of the AMOC-on state by setting $(x_1, x_2) = (1.7, 1.0)$, and consider a randomly chosen trajectory on the Lorenz attractor. Then, we monitor the time when the system tips, if it tips at all during the simulation time, and show the results through the gray shading in Figure 8. To ensure that the initial conditions of the consecutive runs are not correlated, we choose the final condition of the Lorenz system of the previous run, and then run for 5 Lorenz time units.

Forcing with the UPOs is again performed similarly to the analysis of the double-well system. We initialize the system in the vicinity of the AMOC-on state, force it with the UPOs, and perform a bisection in η_1 to find the lowest η_1 for which the system tips. Note that these plots look qualitatively similar to those for the double-well system in Figure 3.

Note that the simulations for Figures 7 and 8 were performed using one initial condition of the response system. We assume that this point remains in the basin of attraction of the AMOC-on state, whenever it exists, on varying the parameter. We have checked and it seems reasonable to assume that the initial point remains in this basin of attraction, even at the saddle node bifurcation.

For increasing a, the effect of the Lorenz forcing plays an increasingly important role leading to earlier or later tipping than the bifurcation point of the unforced Stommel system; the size of the chaotic tipping window increases with increasing a.
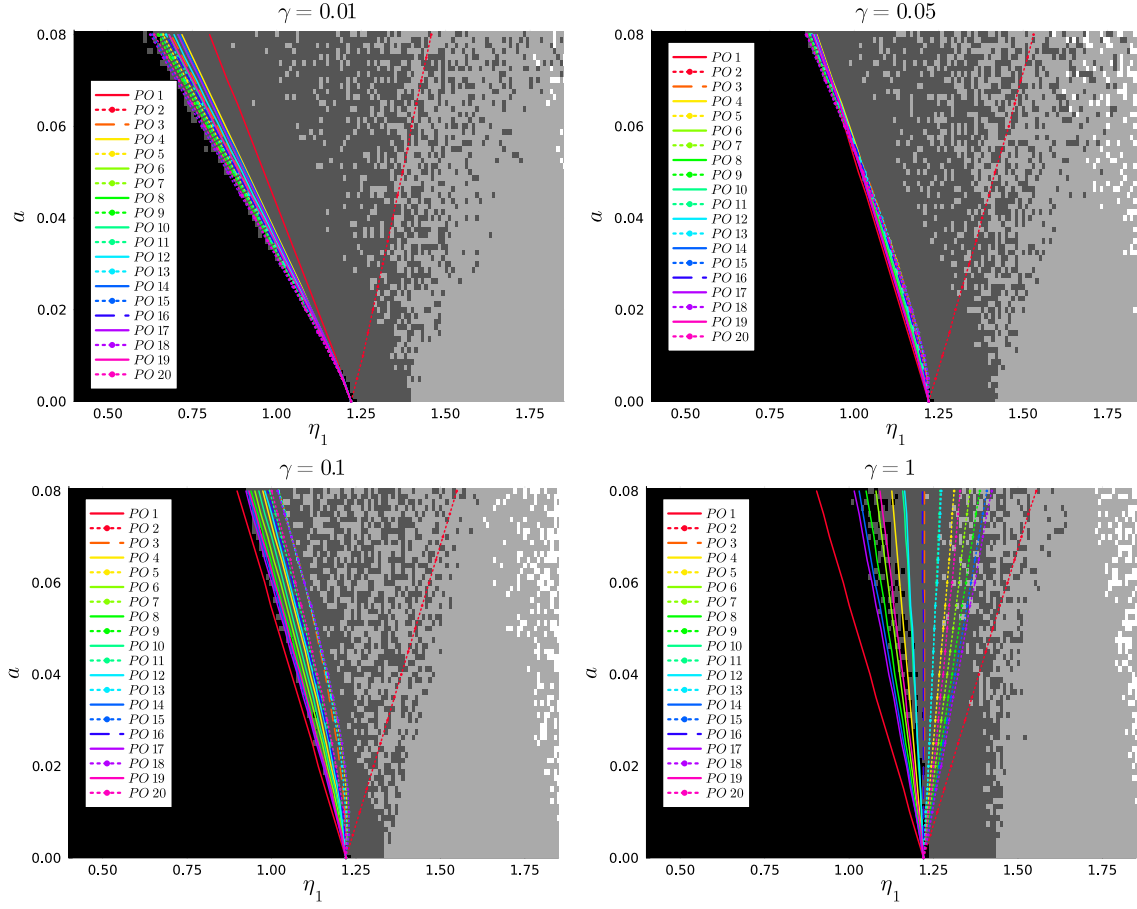
Figure 8: The coloured lines show for each a the lowest value of η_1 for which tipping is observed when forcing the Stommel system 22 with the colour-coded UPO. The system is of the form of equation 6 with $y(t) = y_{UPO_k}$ given by the kth UPO and $\gamma \in (0.01, 0.05, 0.1, 1)$. For each UPO, we fix discrete values of $a \in [0, 0.08]$ with spacing of 0.01 and then perform bisections in $\eta_1 \in (0.4, 1.6)$ to approximate the lowest η_1 up to an accuracy of 5×10^{-3} for which the system initialized in the vicinity of the AMOC-on state at $(x_1, x_2) = (1.7, 1.0)$, tips to the AMOC-off state, i.e. $\Psi < 0.1$. The black, dark grey, and light grey shading are computed analogously to Figure 3. For each combination of (η_1, a), we randomly chose a single orbit of the Lorenz system to force the Stommel system (22) initialized in the vicinity of the AMOC-on state. The Lorenz-initial condition of one run is given by letting the final condition of the previous run evolve for 5 Lorenz-timesteps. The first Lorenz initial condition is given by starting the system at $(y_1, y_2, y_3) = (0.1, 0.1, 25.1)$ and letting it relax to the attractor for 5 Lorenz-timesteps. The gray shadings show tipping for intermediate times. The time intervals corresponding to the different shading colours are given in Table 2 for each value of γ.

19

γ	white	lightgray	darkgray	black
0.01	[0, 0.011)	[0.011, 0.05)	[0.05, 150)	[150, ∞)
0.1	[0, 0.061)	[0.061, 0.22)	[0.22, 150)	[150, ∞)
1	[0, 0.125)	[0.125, 0.7)	[0.7, 150)	[150, ∞)
5	[0, 1.25)	[1.25, 4.0)	[4.0, 150)	[150, ∞)

Table 2: Time intervals during which tipping was observed for each of the different gray shadings in Figure 8, as in Table 1.

The smaller a, the better the linear response theory as discussed in Section 2.1 will describe what happens. Thus, it seems intuitive that for larger a, the ordering of the line by their mean y_1-value for large γ starts to break first, and only for smaller γ also for small values of a.

4 Chaotic tipping with drift: the dynamic tipping window

We turn back to a general one-dimensional additively chaotically forced bistable system (4), where the bifurcation parameter $\eta_r(t)$ is now time-dependent:

$$
\begin{aligned}
\frac{dx}{dt} &= f(x) + \eta_r(t) + a\phi(y) \\
\frac{dy}{dt} &= \gamma g(y).
\end{aligned}
\tag{27}
$$

We define

$$
\eta_r(t) := \eta_0 + rt
\tag{28}
$$

with $r > 0$ and η_0 real constants. The assumptions on the unforced system

$$
\frac{dx}{dt} = f(x) + \eta_r(0)
\tag{29}
$$

are the same as in the time-independent case described after Equation (7). We assume that the system (29) has a bifurcation point η^* that can cause B-tipping. Specifically, suppose that there are two attractors for $\eta^\dagger < \eta_0 < \eta^*$, only one attractor for $\eta_0 > \eta^*$, and that one of the attractors disappears at a saddle-node bifurcation $\eta_0 = \eta^*$. The y-dynamics are assumed to be chaotic.

In the following, we assume $\eta_0 < \eta^*$, and initialize the x-dynamics close to the attractor that would cease to exist for $\eta_0 > \eta^*$. In the limit $r \to 0$, $\eta_r(t)$ would increase adiabatically, and tipping as a result of chaotic forcing would only be possible within the chaotic tipping window described in Section 2 for all finite $a > 0$ and γ fixed.

The forced system responds with a delay compared to the increase in $\eta_r(t)$ and the relaxation to the new attractor corresponding to the new state of $\eta(t)$ needs some time during which $\eta_r(t)$ still increases. For any fixed forcing trajectory, the value of $\eta_r(t_c)$ at time t_c when the threshold of the x-dynamics is crossed increases with increasing r.
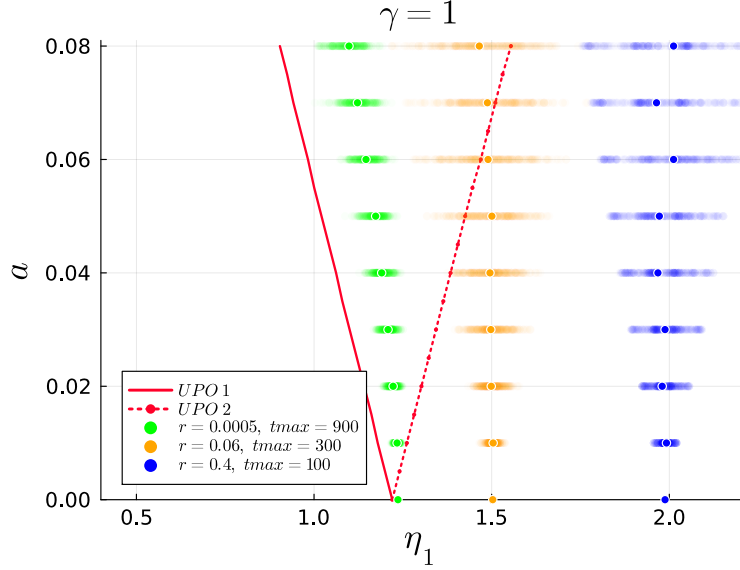
20

Figure 9: The dynamic tipping window: we initialize the x-dynamics in the basin of the AMOC-on state at $(x_1, x_2) = (1.7, 1.0)$, and then do ensembles of runs for three different values of r, a range of values of $a \in [0.0, 0.08]$, and the forcing always initialized by the final condition of the previous run. Thus, we approximate random forcing trajectories. We run the system until time t_c when the system crosses the tipping threshold $\Psi = 0.1$ and store $\eta_r(t_c)$ for each run. For each run, we plot the location of $\eta_r(t_c)$, and for each line of constant a, we show the median tipping location for all three choices of r. The points are plotted slightly transparent such that one can see the distribution of $\eta_r(t_c)$.

Also in the case of time-dependent $\eta_r(t)$, for every r, there exists an η-interval only during which tipping can occur depending on the specific forcing trajectory, but not outside of it. This is due to the boundedness of the y-dynamics and defines the *dynamic tipping window* introduced in [5]. In the limit $r \to 0$, the dynamic tipping window limits to the chaotic tipping window for all finite $a > 0$. The larger r, the more it shifts to larger values of η. Note that the dynamic tipping window depends on the choice of the threshold used to define tipping.

4.1 Example: a ramped Lorenz-Stommel System

We consider the two-dimensional Lorenz-Stommel system (22), replacing the parameter η_1 with a time-dependent parameter $\eta_r(t)$ given by (28) with $\eta_0 = 0.9$. We initialize the x-dynamics in the vicinity of the AMOC-on state at $(x_1, x_2) = (1.7, 1.0)$, and then run ensembles for three different values of r, a range of values of $a \in [0.0, 0.08]$, and the forcing always initialized by the final condition of the previous run. Thus, we approximate random forcing trajectories. We run the system until time t_c when the system crosses the tipping threshold $\Psi = 0.1$ and store $\eta_r(t_c)$ for each run. The results are shown in Figure 9. As expected, we observe that for increasing r, the dynamic tipping window shifts to larger η_1 for all a.

4.2 Phase Dependence of UPO forcing for time-dependent $\eta_1(t)$

Instead of forcing the Stommel system with chaotic trajectories, we could have forced it with the UPOs. In this case the value of $\eta_r(t_c)$ would depend on the initial condition chosen on each UPO. Thus, we would get a range of $\eta_r(t_c)$ for each UPO and forcing strength a. However, in the limits of infinite timescale separation, these ranges should each converge to single values of $\eta_r(t_c)$.

This phenomenon is not to be confused with the *phase tipping* introduced in [1] where a tipping point is only passed because of a combination of the forcing shifting at a certain rate and the system being in a certain phase with respect to its limit cycle. In our setting the system will tip anyway for sufficiently large t as the chaotic forcing is bounded and a finite, and even an untypically stabilizing forcing trajectory could not prevent the x-dynamics from tipping for arbitrarily large $\eta_r(t)$. Thus, the forcing only determines when the system tips and the (de)stabilization of the system should be rather interpreted as an advancing or delaying of the bifurcation.

5 Discussion

In this work, we give an understanding of the chaotic tipping window for chaotically forced ODEs that can exhibit bistability for some parameters. This extends [5] and demonstrates that in the forced ODE system the timescale separation constant γ is vital to understand the relative importance of the mean (for rapid forcing) or extremes (for slow forcing) of the forcing, not just its amplitude. We show that the timescale ratio between the forcing and responding systems strongly affects the forcing behaviour that determines the boundaries of the tipping window; for forcing at similar timescales to the bistable system we expect quite complex behaviour is possible.

The tipping window encodes a great deal of information about the UPOs and system's response. For example, most of the UPOs of the Lorenz system in Figure 11 have similar extrema while their means can vary quite a lot. We recall that finding the end points of the tipping window can be seen as a non-linear version of ergodic optimisation that may be interesting to understand at a more systematic level. Some work has been done to understand bifurcations with bounded noise in terms of set-valued dynamics [20, 19], but it is not clear that this will more easily give information about the tipping windows. We note that we do not give results of relevance to the homogenization limit [17] as this limit requires that $a \approx \sqrt{\gamma}$ and takes the limit $\gamma \to \infty$ - the large forcing amplitude means that the tipping window becomes trivial in this limit.

In the presence of bounded noise and slow drift of a parameter, we show that, not surprisingly, the tipping window becomes dynamic with a delay related to the parameter's drift rate. We did not consider the interplay between the rate of drift and the timescales of forcing and response, but presumably, these will all be important, especially when they are comparable. We also did not consider, for example, the cumulative distribution of tipping times for a drift through a chaotic tipping window, except that some features of this can be inferred from Figure 3 - the shading gives an idea of the time of tipping when parameters reside in these regions. It will be an interesting and potentially useful exercise to quantify this more. As in [5], we expect that an extremely slow drift will be needed for tipping to be likely close to the left boundary of the chaotic tipping window. For more

complex real-world cases where there is a combination of chaotic and slow deterministic forcing there may be a complex interplay of the forcing and response.

Acknowledgements

Data availability

The Julia code to perform the simulations and generate the figures in this paper is available from `https://github.com/raphael-roemer/tipping-windows-and-timescales-2025`.

References

[1] Hassan Alkhayuon, Rebecca C Tyson, and Sebastian Wieczorek. Phase tipping: how cyclic ecosystems respond to contemporary climate. *Proceedings of the Royal Society A*, 477(2254):20210059, 2021.

[2] Hassan M. Alkhayuon and Peter Ashwin. Rate-induced tipping from periodic attractors: Partial tipping and connecting orbits. *Chaos: An Interdisciplinary Journal of Nonlinear Science*, 28(3):033608, Mar 2018.

[3] Vasso Anagnostopoulou and Tobias Jäger. Nonautonomous saddle-node bifurcations: Random and deterministic forcing. *Journal of Differential Equations*, 253(2):379–399, 2012.

[4] Peter Ashwin and Julian Newman. Physical invariant measures and tipping probabilities for chaotic attractors of asymptotically autonomous systems. *The European Physical Journal Special Topics*, 230(16):3235–3248, 2021.

[5] Peter Ashwin, Julian Newman, and Raphael Römer. Contrasting chaotic and stochastic forcing: tipping windows and attractor crises. *SIADS*, 2024.

[6] Peter Ashwin, Clare Perryman, and Sebastian Wieczorek. Parameter shifts for nonautonomous systems in low dimension: bifurcation-and rate-induced tipping. *Nonlinearity*, 30(6):2185, 2017.

[7] Peter Ashwin, Sebastian Wieczorek, Renato Vitolo, and Peter Cox. Tipping points in open systems: bifurcation, noise-induced and rate-dependent examples in the climate system. *Philosophical Transactions of the Royal Society A: Mathematical, Physical and Engineering Sciences*, 370(1962):1166–1184, 2012.

[8] Andrew R. Axelsen, Courtney R. Quinn, and Andrew P. Bassom. Finite-time analysis of crises in a chaotically forced ocean model. *Journal of Nonlinear Sciences*, 34(5):97, 2024.

[9] Nils Berglund and Barbara Gentz. *Noise-induced phenomena in slow-fast dynamical systems: a sample-paths approach.* Springer Science & Business Media, 2006.

[10] Elizabeth Bradley and Ricardo Mantilla. Recurrence plots and unstable periodic orbits. *Chaos: An Interdisciplinary Journal of Nonlinear Science*, 12(3):596–600, 2002.

[11] P. Cvitanović, R. Artuso, R. Mainieri, G. Tanner, and G. Vattay. *Chaos: Classical and Quantum.* Niels Bohr Inst., Copenhagen, 2016.

[12] Ruslan L Davidchack and Ying-Cheng Lai. Efficient algorithm for detecting unstable periodic orbits in chaotic systems. *Physical Review E*, 60(5):6172, 1999.

[13] Henk A. Dijkstra. *Nonlinear climate dynamics.* Cambridge University Press, Cambridge, 2013.

[14] Georg A. Gottwald, Daan Crommelin, and Christian Franzke. Stochastic climate theory. In C. Franzke and T. O'Kane, editors, *Nonlinear and Stochastic Climate Dynamics.* Cambridge University Press, 2017.

[15] K. Hasselmann. Optimal fingerprints for the detection of time-dependent climate change. *Journal of Climate*, 6(10):1957 – 1971, 1993.

[16] Oliver Jenkinson. Ergodic optimization in dynamical systems. *Ergodic Theory and Dynamical Systems*, 39(10):2593–2618, 2019.

[17] David Kelly and Ian Melbourne. Deterministic homogenization for fast–slow systems with chaotic noise. *J. Funct. Anal.*, 272(10):4063–4102, 2017.

[18] Christian Kuehn. *Multiple time scale dynamics*, volume 191. Springer, 2015.

[19] Christian Kuehn, Giuseppe Malavolta, and Martin Rasmussen. Early-warning signals for bifurcations in random dynamical systems with bounded noise. *Journal of Mathematical Analysis and Applications*, 464(1):58–77, 2018.

[20] Jeroen Lamb, Martin Rasmussen, and Christian Rodrigues. Topological bifurcations of minimal invariant sets for set-valued dynamical systems. *Proceedings of the American Mathematical Society*, 143(9):3927–3937, 2015.

[21] Valerio Lucarini and Mickaël D. Chekroun. Theoretical tools for understanding the climate crisis from hasselmann's programme and beyond. *Nat Rev Phys*, 5:744–765, 2023.

[22] I Melbourne and A M Stuart. A note on diffusion limits of chaotic skew-product flows. *Nonlinearity*, 24(4):1361–1367, March 2011.

[23] Paul Ritchie, Özkan Karabacak, and Jan Sieber. Inverse-square law between time and amplitude for crossing tipping thresholds. *Proceedings of the Royal Society A*, 475(2222):20180504, 2019.

[24] Paul So, Edward Ott, Steven J Schiff, Daniel T Kaplan, Tim Sauer, and Celso Grebogi. Detecting unstable periodic orbits in chaotic experimental data. *Physical Review Letters*, 76(25):4705, 1996.

[25] Henry Stommel. Thermohaline convection with two stable regimes of flow. *Tellus*, 13(2):224–230, 1961.

[26] Lai-Sang Young. Generalizations of SRB measures to nonautonomous, random and infinite dimensional systems. *J. Stat. Phys.*, 166:4924–515, 2016.

Name	T	$y_{1,max}$	$y_{1,mean}$	symmetric
UPO1	0.640	11.751	8.050	
UPO2	0.640	-5.135	-8.050	
UPO3	1.545	15.661	-0.073	Y
UPO4	2.285	14.601	2.301	
UPO5	2.285	16.532	-2.301	
UPO6	3.020	14.947	3.456	
UPO7	3.020	17.047	-3.456	
UPO8	3.700	14.957	4.177	
UPO9	3.700	17.000	-4.177	
UPO10	3.825	15.945	1.361	
UPO11	3.825	16.719	-1.361	
UPO12	3.865	15.430	1.325	
UPO13	3.865	16.231	-1.325	
UPO14	4.410	14.757	4.701	
UPO15	4.410	17.602	-4.701	
UPO16	4.635	16.188	-0.001	Y
UPO17	5.110	14.957	5.051	
UPO18	5.110	17.828	-5.051	
UPO19	5.235	15.864	2.970	
UPO20	5.235	17.440	-2.970	

Table 3: Approximate periods T, maximum $y_{1,max}$ and mean $y_{1,mean}$ of the first component of the numerically determined UPOs ($\mathbf{y}(t)$) shown in Figure 11. Note that the symmetric orbits have a mean that is approximately 0.

A   Computation of unstable periodic orbits

We compute the UPOs using the method from [12] as follows. Consider the recurrence matrix M_{rec} of a long trajectory of the Lorenz-63 system defined by:

$$M_{rec}(ij) = \begin{cases} 1, & \text{if } |\mathbf{y}(t_i) - \mathbf{y}(t_j)| \leq \varepsilon \\ 0, & \text{otherwise.} \end{cases}$$

An example is shown in figure 10. Then, from each stripe in the recurrence matrix, we choose the candidate $M_{rec}(ij)$ with the smallest recurrence distance $|\mathbf{y}(t_i) - \mathbf{y}(t_j)|$. This provides a list of approximated periodic orbits.

Many of the identified UPOs can now either be directly identified with each other, or they are identical after a rotation (i.e. they are identical if one applies the transformation $(y_1, y_2, y_3) \mapsto (-y_1, -y_2, y_3)$) or they are similar in the sense that a UPO is run through several times and thus has a length that is an integer multiple of its actual length. Thus, we identify many of the previously collected candidates for periodic orbits with each other. We illustrate a number of the resulting UPOs computed for the Lorenz attractor in Figure 11 and list some properties of these UPOs in Table 3.
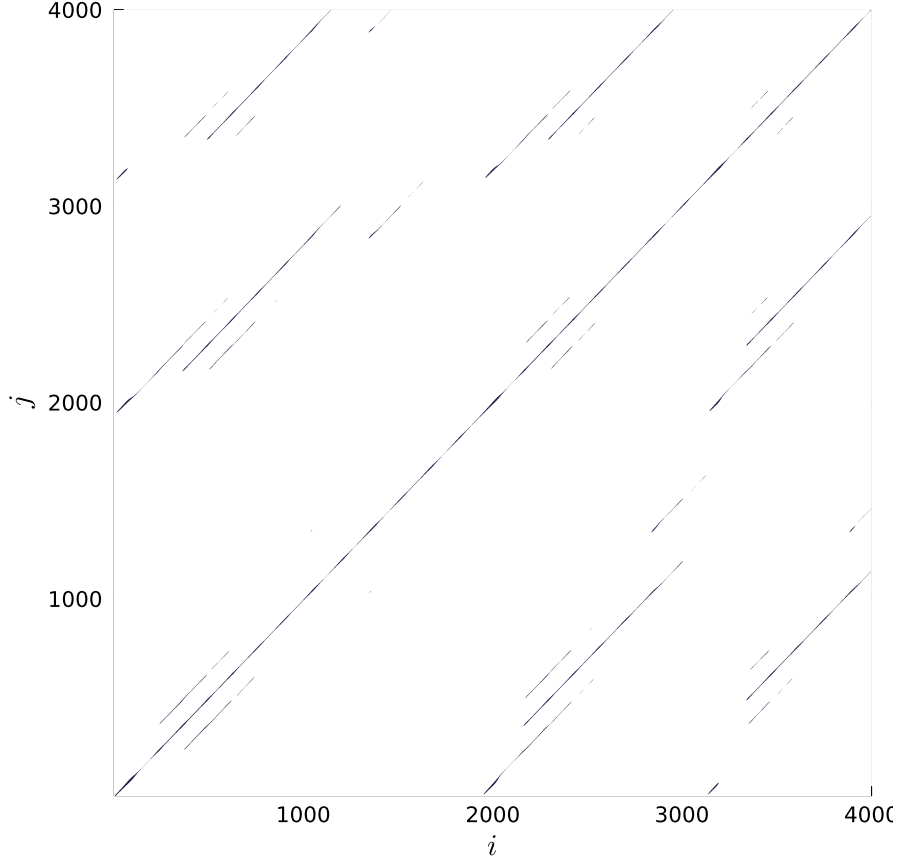
Figure 10: The first 4000 timesteps of the recurrence matrix $M_{rec}(i, j)$ for a numerically integrated trajectory of the Lorenz system (24) starting at $(y_1, y_2, y_3) = (0.05, 0.05, 25.05)$. The i and j axes refer to timestep number t_i and t_j. Black indicates a recurrence where $|\mathbf{y}(t_i) - \mathbf{y}(t_j)| \leq \varepsilon = 0.9$. In each of the black stripes, we search for a pair (i, e) with closest recurrence and approximate orbit closure and use this as the candidate for a point on the UPO.
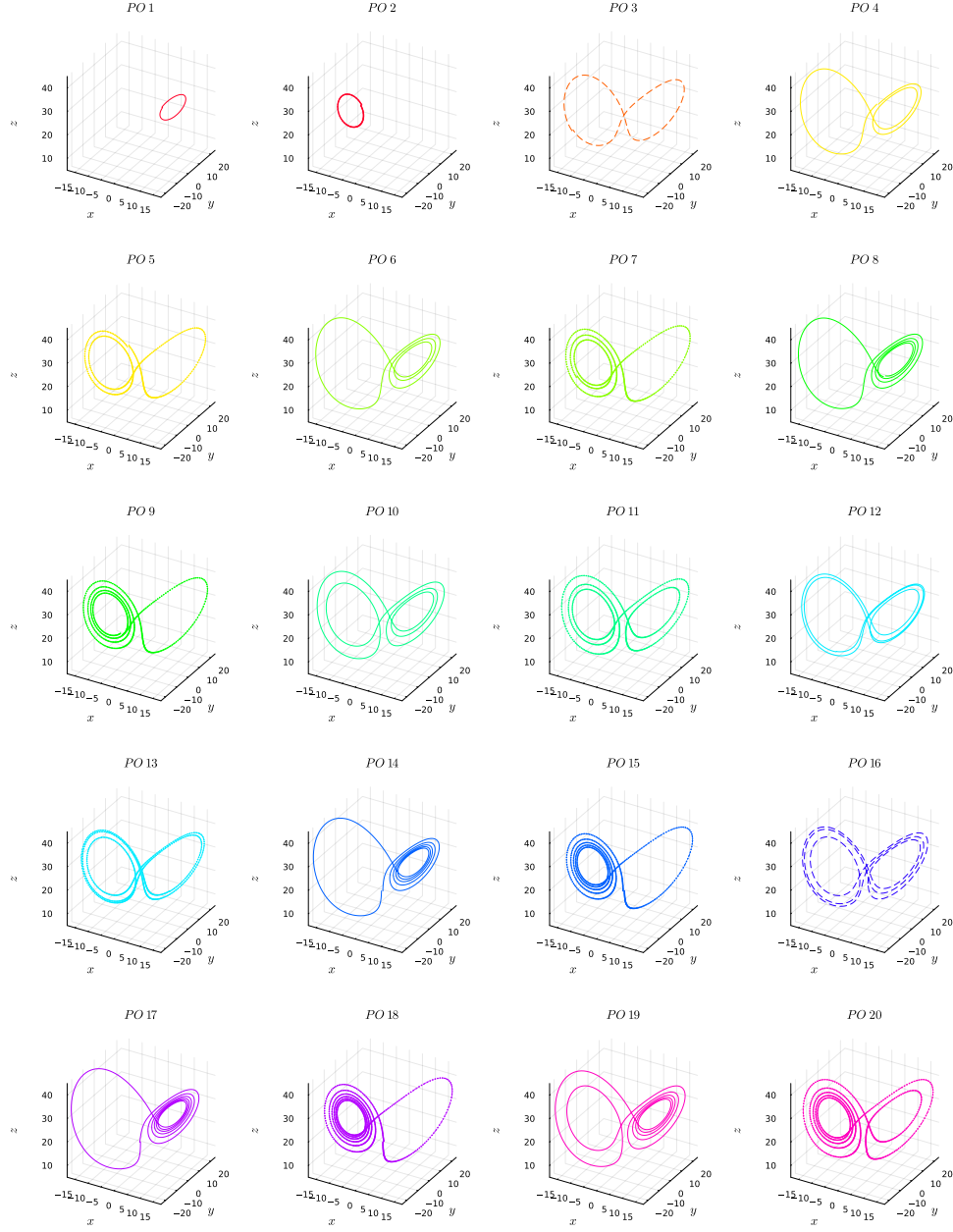
27

Figure 11: Numerical approximations of a set of low period UPOs of the Lorenz system within the Lorenz attractor, computed using the method of recurrences from a long chaotic trajectory on the Lorenz attractor. Dashed lines show axis-symmetric orbits. Orbits with the same colour are symmetrically related.